JACS
JOURNAL OF THE AMERICAN CHEMICAL SOCIETY
Article
pubs.acs.org/JACS

Single-Crystal X-ray Diffraction Study of Three Yb@C_{82} Isomers Cocrystallized with Ni^{II}(octaethylporphyrin)

Mitsuaki Suzuki,[†] Zdenek Slanina,[†] Naomi Mizorogi,[†] Xing Lu,*[,†,‡] Shigeru Nagase,*[,§] Marilyn M. Olmstead,*[,∥] Alan L. Balch,*[,∥] and Takeshi Akasaka*[,†]

[†]Life Science Center of Tsukuba Advanced Research Alliance, University of Tsukuba, Tsukuba, Ibaraki 305-8577, Japan

[‡]State Key Laboratory of Materials Processing and Die & Mold Technology, College of Materials Science and Engineering, Huazhong University of Science and Technology (HUST), 1037 Luoyu Road, Wuhan 430074, China

[§]Fukui Institute for Fundamental Chemistry, Kyoto University, Kyoto 606-8103, Japan

[∥]Department of Chemistry, University of California, One Shields Avenue, Davis, California 95616, United States

Supporting Information

ABSTRACT: Single crystals of three soluble Yb@C_{82} isomers, namely, Yb@C_2(5)-C_{82}, Yb@C_s(6)-C_{82}, and Yb@C_{2v}(9)-C_{82}, cocrystallized with Ni^{II}(octaethylporphyrin), allowed accurate crystallographic elucidation of their molecular structures in terms of both cage symmetry and metal location. Multiple metal positions were found in all these isomers, but the major metal sites were found in some specific regions within these cages. Specifically, the Yb^{2+} ion prefers to reside close to a hexagonal ring in Yb@C_2(5)-C_{82} and Yb@C_{2v}(9)-C_{82} but a [5,6,6]-junction carbon atom in Yb@C_s(6)-C_{82}. Theoretical calculations at the B3LYP level revealed that these metal positions all correspond to energy minima from the electrostatic potential maps and give rise to the most stable configurations of these Yb@C_{82} isomers. Furthermore, it is noteworthy that this is the first report on X-ray crystallographic studies of such metallofullerenes with the popular C_{2v}(9)-C_{82} encapsulating a divalent metal ion, described as M^{2+}@[C_{2v}(9)-C_{82}]$^{2-}$.

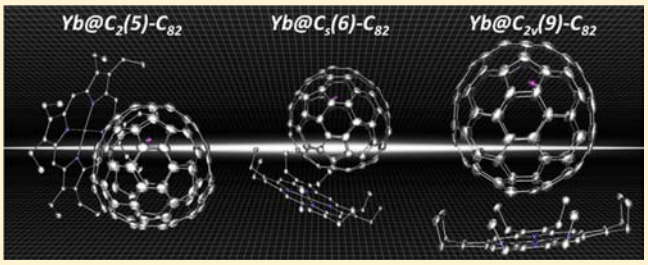

INTRODUCTION

Metal doping of the interior of fullerene cages generates a new class of hybrid molecules with unique structures, novel properties, and potential applications in such fields as photovoltaics, biomedicine, and materials science.[1,2] As the simplest examples of endohedral metallofullerenes (EMFs), such compounds containing only one metal ion have been of particular interest throughout the research era of EMFs. Since the first report on the solvent extraction of EMFs from raw soot,[3] M@C_{82}-type (M = Sc, Y, lanthanide) species have attracted wide attention because of their relatively high yield and good solubility in common organic solvents.[4] In these species, three electrons are transferred from the internal metal to the fullerene cage, while strong electrostatic interactions attract the metal ions to the walls of the fullerene cage.[5]

Meanwhile, structural elucidation of EMFs is of high importance because their intrinsic properties are highly susceptible to these structural issues. NMR spectroscopy has been widely used to characterize the cage structures of EMFs. For example, the cage symmetry of the major isomer of the prototypical La@C_{82} was revealed to be C_{2v}(9)-C_{82} by ^{13}C NMR spectrometry performed on its anion, and the minor La@C_{82} isomer was found to be La@C_s(6)-C_{82} in combination with theoretical results.[6] Similar methodology has also been applied to other M@C_{82} isomers to determine their cage structures. It was very interesting to find that even when La is replaced with a different rare-earth metal (e.g., Y, Ce, Pr, or Gd), the EMFs always utilize the C_{2v}(9)-C_{82} cage, sometimes with M@C_s(6)-C_{82} also being observed.[7] Again, all these compounds feature the transfer of three electrons from the metal to the cage.

Nonetheless, the NMR technique generally provides valuable information about the cage symmetry but not the metal position inside the fullerene cage. Subsequently, many derivatives of M@C_{2v}(9)-C_{82} particularly suitable for single-crystal growth have also been obtained. Accordingly, most of them have been structurally characterized by single-crystal X-ray diffraction (XRD) crystallographic studies, which have produced valuable information about the metal position and metal−cage interactions in these prominent molecules.[8] Alternatively, the motion of the spherical EMF molecules in the crystal lattice can also be stopped by cocrystallization with a metal porphyrin in order to obtain crystals with sufficient order for XRD analysis. This methodology has been widely adopted to get structural information on fullerenes and EMFs. More than 60 examples of EMFs or empty fullerenes cocrystallized with metal porphyrins have been reported, but most of the

Received: September 2, 2012
Published: October 22, 2012

   dx.doi.org/10.1021/ja308706d | J. Am. Chem. Soc. 2012, 134, 18772−18778

Table 1. Crystal Data for the Three Yb@C_{82} Isomers Cocrystallized with Ni^{II}(OEP)

	Yb@C_s(6)-C_{82}·Ni^{II}(OEP)·2(benzene)	Yb@C_2(5)-C_{82}·Ni^{II}(OEP)·2(benzene)	Yb@C_{2v}(9)-C_{82}·Ni^{II}(OEP)·2(benzene)
isomer label[12]	I	II	III
formula	$C_{130}H_{56}N_4NiYb$	$C_{130}H_{56}N_4NiYb$	$C_{130}H_{56}N_4NiYb$
formula weight	1905.54	1905.54	1905.54
color, habit	black, block	black, block	black, block
crystal system	triclinic	monoclinic	monoclinic
space group	$P\bar{1}$	$C2/m$	$C2/m$
a (Å)	14.613(2)	25.335(3)	25.264(4)
b (Å)	14.816(2)	15.045(2)	15.169(2)
c (Å)	19.934(3)	19.813(3)	19.869(3)
α (deg)	86.130(2)	90.00	90.00
β (deg)	86.023(2)	94.270(2)	95.078(2)
γ (deg)	61.312(2)	90.00	90.00
V (Å^3)	3774.2(11)	7531.3(17)	7584(2)
Z	2	4	4
radiation (λ/Å)	fine-focus sealed tube (0.71073)	fine-focus sealed tube (0.71073)	fine-focus sealed tube (0.71073)
unique data (R_{int})	46939 (0.0309)	47691 (0.0280)	48930 (0.0377)
obsd data [$I > 2\sigma(I)$]	19878	10460	10980
R_1[a] (obsd data)	0.0636	0.0690	0.0857
wR_2[b] (all data)	0.1762	0.2002	0.2421

[a]For data with $I > 2\sigma(I)$. $R_1 = \sum||F_o| - |F_c||/|\sum F_o|$. [b]For all data. $wR_2 = \{\sum[w(F_o^2 - F_c^2)^2]/\sum[w(F_o^2)^2]\}^{1/2}$.

studies have focused on such compounds with a metal cluster inside or on large cages such as C_{84}, C_{90}, or C_{94} containing a single metal ion.[9] For cocrystals of M@C_{82}, very few reports are available. La@C_{2v}(9)-C_{82} and Gd@C_{2v}(9)-C_{82} are the first two compounds of M@C_{82} whose structures were determined by XRD crystallography using the cocrystallization method.[10] The results showed that the single metal ion tends to reside under a hexagonal ring along the two-fold axis. Very recently, three isomers of Sm@C_{82}, namely, Sm@C_2(5)-C_{82}, Sm@C_s(6)-C_{82}, and Sm@C_{3v}(7)-C_{82}, were also structurally characterized with XRD crystallography through the cocrystal formation with Ni^{II}(OEP), where OEP is the dianion of 2,3,7,8,12,13,17,18-octaethylporphyrin.[11] In contrast to the nearly fixed positions of trivalent La^{3+} and Gd^{3+} ions in the C_{2v}(9)-C_{82} cage, multiple metal positions were observed for the divalent Sm^{2+} cation in these C_{82} cages, indicating a dynamic metal ion inside. However, it is not conclusive whether the different motional behaviors of the trivalent (La^{3+} and Gd^{3+}) and divalent (Sm^{2+}) ions in these C_{82} cages are caused by their different electronic configurations or by the different cage symmetries.

We recently obtained a series of typical divalent EMFs containing an ytterbium atom, which donates two valence electrons to the surrounding cage. By means of ^{13}C NMR spectroscopy in combination with computational studies, the cage symmetries of these EMFs were established as Yb@C_{2v}(3)-C_{80}, Yb@C_2(5)-C_{82}, Yb@C_s(6)-C_{82}, Yb@C_{2v}(9)-C_{82}, Yb@C_2(11)-C_{84}, Yb@C_2(13)-C_{84}, and Yb@C_1(12)-C_{84}, respectively.[12] As mentioned above, however, it was not possible to determine the metal position in these cages from the NMR results. Accordingly, single-crystal XRD measurements were attempted. The first crystallographic study of a Yb EMF was conducted on Yb@C_{2v}(3)-C_{80} through cocrystal formation with Ni(OEP), and the results revealed that the metal ion is localized under a hexagonal ring that is off to the side of the axis of symmetry.[13] In this article, we report a systematic X-ray crystallographic study of the structures of the three Yb@C_{82} isomers mentioned above, namely, Yb@C_s(6)-C_{82}, Yb@C_2(5)-C_{82}, and Yb@C_{2v}(9)-C_{82}.

EXPERIMENTAL SECTION

Procedures for the synthesis, isolation, and spectroscopic characterization of the three Yb@C_{82} isomers followed those reported in previous studies,[12] and the data are presented in Figures S1−S3 in the Supporting Information.

Black crystalline rods of the three isomers of Yb@C_{82} with Ni^{II}(OEP) were obtained by layering a benzene solution of Ni^{II}(OEP) on top of a CS_2 solution of the appropriate EMF in a glass tube (φ = 7 mm) at 273 K. It was interesting to find that only benzene molecules were present in the crystal lattice, while CS_2 molecules were absent. This is most probably due to the high volatility of CS_2. XRD measurements were performed at 90 K on a Bruker AXS instrument equipped with an Apex II CCD detector with Mo Kα radiation (λ = 0.71073 Å). The multiscan method was used for absorption corrections. The structures were solved by direct methods and refined using SHELXL 97.[14] Crystal data for these isomers are given in Table 1.

COMPUTATIONAL DETAILS

Density functional theory (DFT) calculations were conducted using the Gaussian 09 program.[15] As in ref 12, the molecular structures were first optimized at the B3LYP/3-21G~CEP level [B3LYP density functional with the 3-21G basis set for C atoms and the CEP-4G basis set with the CEP effective core potential (ECP) for Yb] and then reoptimized at the B3LYP/6-31G*~SDD level (B3LYP functional with the 6-31G* basis set for C and the SDD basis set with the SDD ECP for Yb).[16] Energy minima were checked using B3LYP/3-21G~CEP vibrational analysis.[16] The electrostatic potential maps were calculated at the B3LYP/6-31G* level.[16] The complexes of Yb@C_{82} with Ni^{II}(OEP) were optimized at the M06-2X/3-21G~SDD level.[16h]

RESULTS AND DISCUSSION

Single-Crystal X-ray Structural Analysis of Yb@C_2(5)-C_{82}·Ni^{II}(OEP)·2(benzene). As commonly encountered in cocrystals formed from EMFs and Ni(OEP), this compound crystallizes in the monoclinic space group $C2/m$ (Table 1). Thus, the asymmetric unit contains half of the Ni^{II}(OEP) molecule and two halves of the C_2(5)-C_{82} cage.[2f,17] The fully ordered nickel porphyrin is present on the crystallographic mirror that bisects N1, Ni1, and N3 (Figure 1), so an intact Ni^{II}(OEP) molecule was readily obtained by combining the

dx.doi.org/10.1021/ja308706d | J. Am. Chem. Soc. 2012, 134, 18772−18778

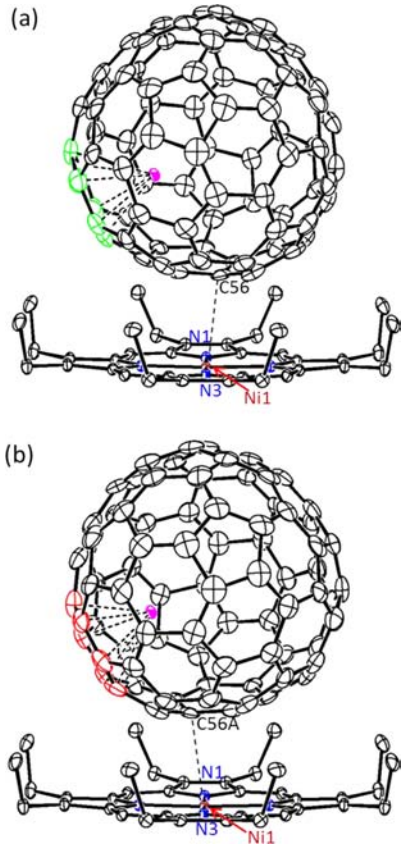

Figure 1. ORTEP drawings of Yb@$C_2(5)$-C_{82}·Ni^{II}(OEP) with 30% thermal ellipsoids. Only the major metal site (Yb1 with 0.18 occupancy) is shown in both views, while solvent molecules, the minor metal positions, and H atoms have been omitted for clarity. The crystallographic mirror plane bisects N1, Ni1, and N3 and lies perpendicular to the plane of the page. Symmetry code: A = $+x$, $-y$, $+z$. The cages shown in (a) and (b) are mutual mirror images. In both structures, Yb1 is located close to a hexagonal carbon ring. C56 and C56A are the cage carbon atoms nearest to Ni^{II}(OEP).

existing half-molecule with its mirror image. However, the chiral $C_2(5)$-C_{82} cage resides in such a way that its two-fold axis is not coincident with the crystallographic mirror plane. As a result, a complete C_{82} cage was finally obtained by combining one of the halves of the fullerene cage with the mirror image of the other. Accordingly, the occupancies of the two cage orientations are 0.50.

Figure 1 shows the two cage orientations and their relationships to the Ni^{II}(OEP) molecule. Only the major ytterbium site (Yb1 with 0.18 occupancy; see below) is shown. The nearest cage−Ni contacts involve C56 or C56A with a distance of 2.79(3) Å. It was interesting to find that the major metal site in both cage orientations is under a hexagonal ring, highlighted in green for the cage orientation shown in Figure 1a and in red for the other orientation shown in Figure 1b. The Yb−cage distances in the two configurations are similar: 2.43(2)−2.64(1) Å for the green-highlighted part and 2.33(1)−2.81(1) Å for the red-highlighted part. This implies that the divalent metal still prefers to stay close to a cage hexagon in $C_2(5)$-C_{82}. Unfortunately, there was no way to determine crystallographically whether either or both of these two locations are occupied. However, theoretical calculations (see below) revealed that the site shown in Figure 1a lies at an energy minimum. Surprisingly, the relationship between Yb@$C_2(5)$-C_{82} and Ni^{II}(OEP) (Figure 1a) is very similar to the situation in the Sm@$C_2(5)$-C_{82}·Ni^{II}(OEP) system.[11] Indeed, Yb@$C_2(5)$-C_{82}·Ni^{II}(OEP)·2(benzene) is isostructural with Sm@$C_2(5)$-C_{82}·Ni^{II}(OEP)·2(benzene). It is interesting to note that the metal ion positions in the two crystals are also remarkably similar.[11]

Inside the cage, there are five sites for the ytterbium cation, with occupancies of 0.18 for Yb1, 0.15 for Yb2, 0.12 for Yb3, 0.03 for Yb4, and 0.02 for Yb5. Figure 2 shows a drawing of one

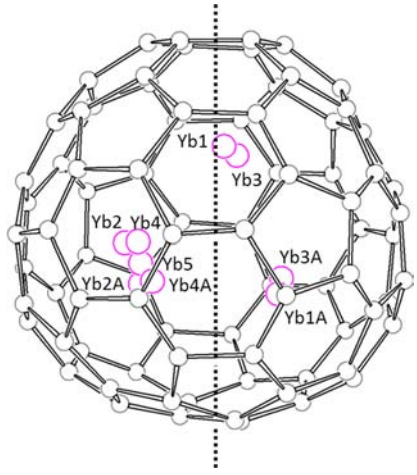

Figure 2. Diagram showing all of the metal sites in Yb@$C_2(5)$-C_{82}. The dotted line illustrates the noncrystallographic two-fold axis of $C_2(5)$-C_{82}.

cage orientation containing all of the metal positions (sites labeled with "A" were generated by symmetry operations). It is evident that the metals are gathered into three groups inside the cage, each near a hexagonal ring.

Single-Crystal X-ray Structural Analysis of Yb@$C_s(6)$-C_{82}·Ni^{II}(OEP)·2(benzene). Fortunately, this crystal belongs to the triclinic space group $P\bar{1}$, in which an intact pair of the EMF and Ni^{II}(OEP) molecules are present together with two benzene molecules filled in the unit cavities. This has the advantage over the monoclinic space group $C2/m$ in providing more reliable information about the metal position and metal−cage relationship. There are two orientations of the $C_s(6)$-C_{82} cage with fractional occupancies of 0.57 and 0.43. Figure 3 shows the major and minor cage orientations and their relationships to the Ni^{II}(OEP) molecule. Only the most abundant metal site (Yb1 with 0.35 occupancy; see below) is shown in these two drawings. The shortest C_{cage}−Ni distances are 2.75(1) Å for the major cage and 2.83(2) Å for the minor one. In both cage orientations, Yb1 resides under a [5,6,6]-junction carbon. The shortest Yb1−cage distances range from 2.37(1) to 2.990(4) Å for the major cage orientation (green part in Figure 3a) and from 2.28(2) to 3.04(2) Å for the minor cage orientation (red part in Figure 3b).

Within these cages, there are 11 ytterbium sites at general positions. The major site (Yb1) has a fractional occupancy of 0.35, and the other minor sites have fractional occupancies ranging from 0.13 to 0.02. Figure 4 shows the major cage encapsulating all 11 metal sites. These ytterbium positions are gathered into three specific groups inside the $C_s(6)$-C_{82} cage. In one area, Yb2 and Yb8 are very close and approach a [5,6,6]-junction, while in another place, Yb7 and Yb10 are near a different [5,6,6]-junction that is symmetrically related to the

dx.doi.org/10.1021/ja308706d | J. Am. Chem. Soc. 2012, 134, 18772−18778

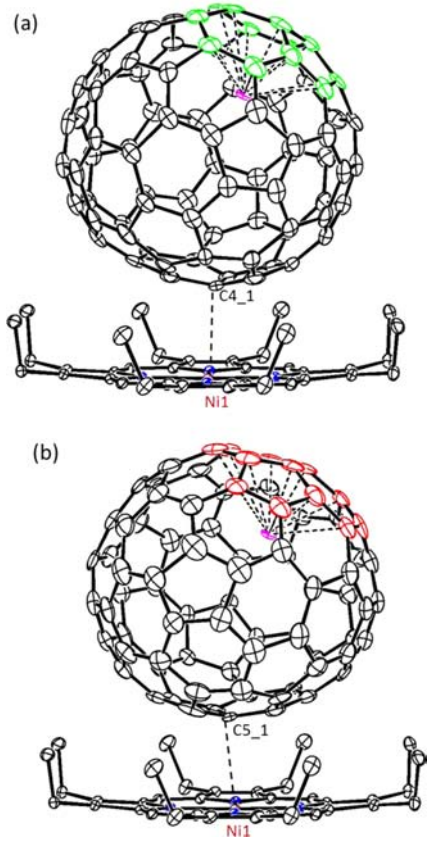

Figure 3. ORTEP drawings of Yb@C_s(6)-C_{82}·Ni^{II}(OEP) with 30% thermal ellipsoids showing the relationship between the fullerene cage and Ni^{II}(OEP) in Yb@C_s(6)-C_{82}·Ni^{II}(OEP)·2(benzene). There are two orientations of the C_s(6)-C_{82} cage with fractional occupancies of (a) 0.57 and (b) 0.43. Only the major ytterbium ion site (Yb1 with 0.35 fractional occupancy) is shown in each cage. For clarity, the benzene molecules, minor metal sites, and H atoms have been omitted.

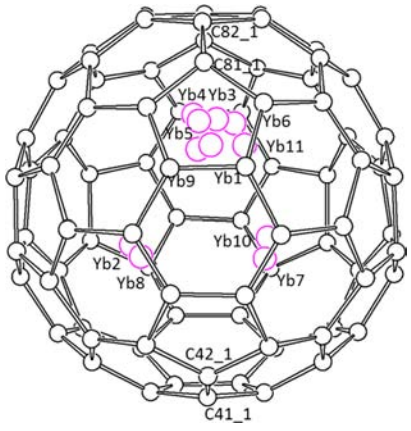

Figure 4. Diagram showing all of the ytterbium sites in the major C_s(6)-C_{82} cage orientation with 0.57 occupancy. The symmetric mirror plane of the C_s(6)-C_{82} passes through C41_1, C42_1, C81_1, and C82_1 and is perpendicular to the page.

previous one. For the other metal sites where Yb1, Yb3, Yb4, Yb5, Yb6, Yb9, and Yb11 reside with a summed occupancy of 0.74, a [6,6]-bond junction or a [5,6,6]-junction closest to the symmetry mirror is more preferred by the metal ion. The location of the major metal ion site is in agreement with the electrostatic potential valley in $[C_s(6)\text{-}C_{82}]^{2-}$ (see below) and the optimized structure of Yb@C_s(6)-C_{82} (Figure S4 in the Supporting Information). This crystallographic study indicates that Yb^{2+} ion might jump from the major site to the other sites corresponding to Yb2, Yb8, Yb7, and Yb10 or vice versa.

Single-Crystal X-ray Structural Analysis of Yb@C_{2v}(9)-C_{82}·Ni^{II}(OEP)·2(benzene). Again the crystal belongs to the monoclinic space group $C2/m$, where half of the Yb@C_{2v}(9)-C_{82} molecule and half of a Ni^{II}(OEP) are present. Both the cage and the internal metal are disordered. Interestingly, three cage orientations are observed in this crystal. The major orientation of the C_{2v}(9)-C_{82} cage with 0.46 occupancy exists with one of its two symmetry planes coincident with the crystallographic mirror plane. Thus, an entire cage can be assembled by combining its mirror image with the existing half. The two minor cage orientations reside at common sites. Each site has an occupancy of 0.27. Figure 5 shows the major metal ion site (Yb1, 0.18 occupancy), the three cage orientations, and their relationships to Ni^{II}(OEP). The shortest distances between a carbon ion of Yb@C_{2v}(9)-C_{82} and the nickel ion in Ni^{II}(OEP) is 2.79(3) Å, which is similar to the values of 2.78(2) Å found in La@C_{2v}(9)-C_{82}·Ni^{II}(OEP) and 2.784(8) Å in Gd@C_{2v}(9)-C_{82}·Ni^{II}(OEP). In the major cage orientation (Figure 5a), Yb1 is located under a hexagonal ring but slightly away from the two-fold axis of the C_{2v}(9)-C_{82} cage, as previously observed for the trivalent Gd^{3+} ion in Gd@C_{2v}(9)-C_{82}.[10b] The distances between Yb1 and the carbon atoms of the nearest hexagonal ring (green part in Figure 5a) vary from 2.30(2) to 2.77(2) Å (Figure 5a). In the two minor cage orientations, however, Yb1 is situated under two different [5,6]-bond junctions with similar Yb−cage distances.

Inside the cage, eight metal sites were detected; three sites (Yb1, Yb5, Yb6) exist on the crystallographic mirror plane, and the remaining five are on general positions. Accordingly, five additional metal ion sites are generated by reflection. The major site, Yb1, is on the crystallographic mirror plane and has a fractional occupancy of 0.18. The other sites have occupancies in the range from 0.12 to 0.02. Figure 6 shows the major cage orientation containing all 13 of these metal ion sites. As was the case with Yb@C_2(5)-C_{82}, crystallographic results alone cannot determine the true metal ion position in Yb@C_{2v}(9)-C_{82}. However (see below), the calculated electrostatic potential valley of $[C_{2v}(9)\text{-}C_{82}]^{2-}$ and the optimized structure of Yb@C_{2v}(9)-C_{82} indicate that the Yb^{2+} ion is located under the hexagon along the two-fold axis of the C_{2v}(9)-C_{82} cage (see Figure 5a). Similar results regarding the position of the metal ion were obtained for La@C_{2v}(9)-C_{82} and Gd@C_{2v}(9)-C_{82}, where computational and experimental work indicated that the metal ion (La^{3+} or Gd^{3+}) is also positioned beneath a hexagon near the two-fold axis.[10] For Yb@C_{2v}(9)-C_{82}, there is no metal site close to the [6,6]-bond junction, which was the location proposed for the divalent Eu^{2+} ion in Eu@C_{2v}(9)-C_{82} on the basis of synchrotron radiation powder diffraction coupled with Rietveld treatment of the diffraction data and the maximum entropy method.[18] All of these results suggest that Eu@C_{2v}(9)-C_{82} may also have a normal metal ion placement analogous to the situation in La@C_{2v}(9)-C_{82}, Gd@C_{2v}(9)-C_{82}, and Yb@C_{2v}(9)-C_{82}.

Computational Studies. For C_{82}, there are nine isomers obeying the isolated pentagon rule (IPR).[19] In an earlier report on the NMR characterizations of Yb@C_{82}, we computed the relative stabilities for the three C_2-C_{82} cages and the three C_s-C_{82} cages.[12] In this work, we performed DFT calculations on

dx.doi.org/10.1021/ja308706d | J. Am. Chem. Soc. 2012, 134, 18772−18778

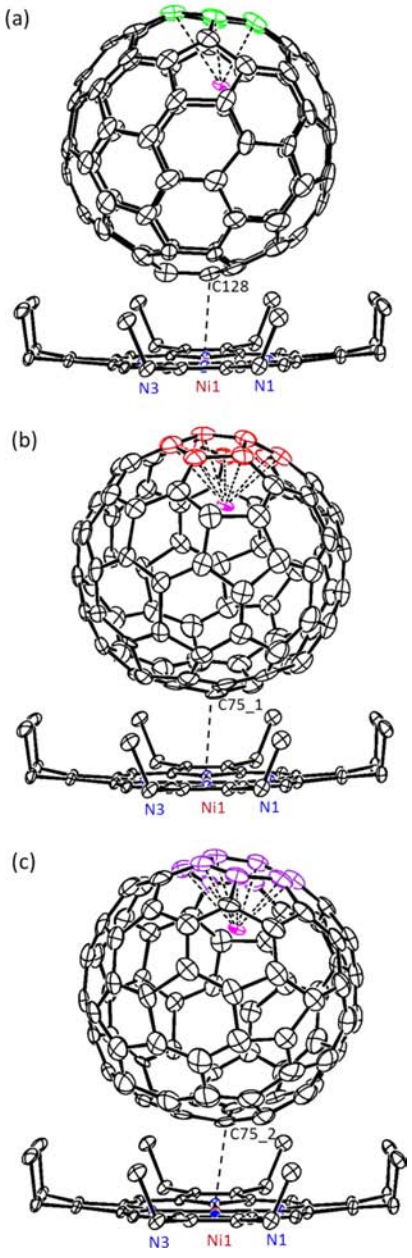

Figure 5. ORTEP drawings of Yb@C_{2v}(9)-C_{82}·Ni^{II}(OEP) with 30% thermal ellipsoids: (a) the major cage orientation, with 0.46 occupancy; (b, c) the two minor cage orientations, each with 0.27 occupancy. Only the major metal site (Yb1 with 0.18 occupancy) is shown in each drawing. A crystallographic mirror plane bisects Ni1, N1, N3, and Yb1 and lies parallel to the page. For clarity, the benzene molecules, minor metal ion sites, and H atoms have been omitted.

the relative stabilities of all nine of these IPR-obeying C_{82} isomers encapsulating an Yb^{2+} ion at the B3LYP/6-31G*∼SDD level. Table 2 contains the calculation results. It is evident that the most stable Yb@C_{82} isomer is Yb@C_{2v}(9)-C_{82}, followed by Yb@C_s(6)-C_{82} and Yb@C_2(5)-C_{82}, all of which were obtained experimentally and structurally confirmed by single-crystal XRD measurements in this work. Furthermore, we found that all of these isomers have relatively large HOMO−LUMO gaps, consistent with their closed-shell electronic configurations.

To pursue theoretical support for the multiple metal ion (Yb^{2+}) positions found in the XRD measurements, we computed the electrostatic potential maps of $[C_2(5)\text{-}C_{82}]^{2-}$,

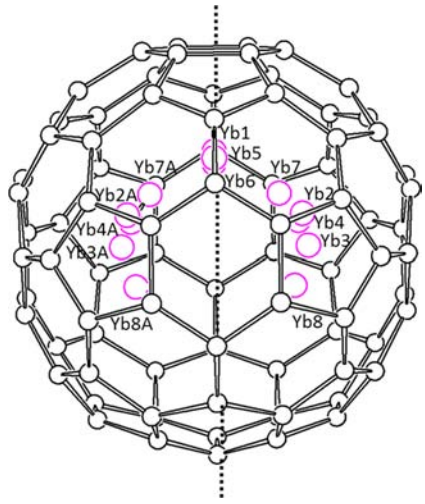

Figure 6. Diagram showing all of the ytterbium sites in the major C_{2v}(9)-C_{82} cage orientation with 0.47 occupancy. A crystallographic mirror plane is aligned vertically across the center of the molecule and perpendicular to the page, coincident with one of the two symmetry planes of C_{2v}(9)-C_{82}. Symmetry code: A = +*x*, 1−*y*, +*z*.

Table 2. Relative Energies and HOMO−LUMO Gaps of Nine IPR-Satisfying Yb@C_{82} Isomers Calculated at the B3LYP/6-31G*∼SDD level

isomer	Δ*E* (kcal/mol)	HOMO−LUMO gap (eV)
Yb@C_2(1)-C_{82}	18.21	1.61
Yb@C_s(2)-C_{82}	24.96	1.13
Yb@C_2(3)-C_{82}	17.41	1.21
Yb@C_s(4)-C_{82}	14.66	1.29
Yb@C_2(5)-C_{82}	4.20	1.64
Yb@C_s(6)-C_{82}	1.86	1.37
Yb@C_{3v}(7)-C_{82}	9.53	1.90
Yb@C_{3v}(8)-C_{82}	11.16	1.10
Yb@C_{2v}(9)-C_{82}	0.00	1.40

$[C_s(6)\text{-}C_{82}]^{2-}$, and $[C_{2v}(9)\text{-}C_{82}]^{2-}$ at the B3LYP/6-31G* level. As shown in Figure 7, the electrostatic potential values are all negative (i.e., stabilization for cations) inside these three C_{82} cages. Interestingly, an electrostatic potential valley was found to reside close to a specific region in each of these cages, and the Yb^{2+} ion should be most stabilized when it falls into the bottom of this valley. Specifically, the minimum of the electrostatic potentials in $C_2(5)\text{-}C_{82}$ is located above a hexagonal carbon ring along the two-fold axis. The minimum in $C_s(6)\text{-}C_{82}$ is close to a [5,6,6]-bond junction across the symmetric mirror plane, while in Yb@C_{2v}(9)-C_{82}, the minimum was found to be under a hexagon along the two-fold axis.

Indeed, when the Yb^{2+} ion was placed inside these three cages, we found that the most stable structures corresponded to the electrostatic potential minima. The optimized structures of Yb@C_2(5)-C_{82}, Yb@C_s(6)-C_{82}, and Yb@C_{2v}(9)-C_{82} are shown in Figure S4 in the Supporting Information. It is noteworthy that in Yb@C_{2v}(9)-C_{82}, the configuration with Yb^{2+} slightly off the symmetric axis is 0.189 kcal/mol more stable than that with the Yb^{2+} cation right along the axis. This shows perfect agreement with the X-ray results (cf. Figure 5a). Our theoretical work also confirmed that the cocrystal formation of the EMFs with Ni^{II}(OEP) does not change the metal position significantly. As shown in Figure S5 in the Supporting

dx.doi.org/10.1021/ja308706d | J. Am. Chem. Soc. 2012, 134, 18772−18778

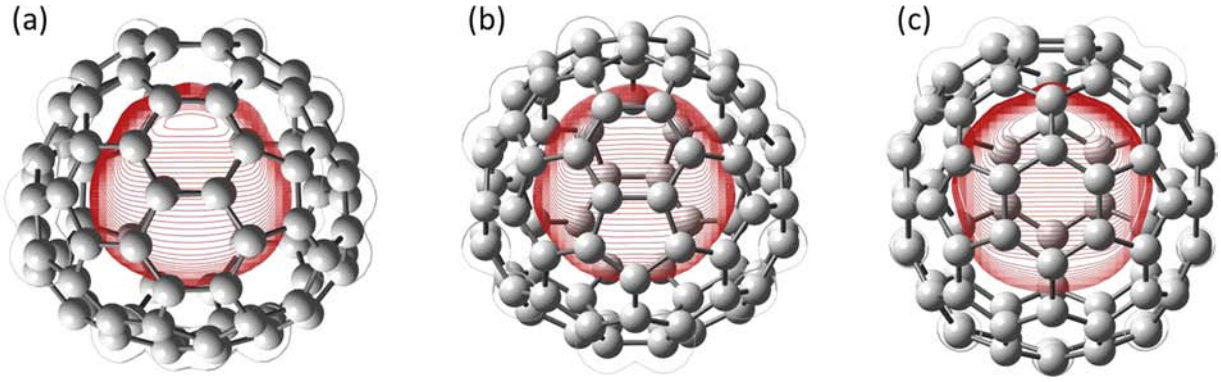

Figure 7. Electrostatic potential maps of (a) $[C_2(5)\text{-}C_{82}]^{2-}$, (b) $[C_s(6)\text{-}C_{82}]^{2-}$, and (c) $[C_{2v}(9)\text{-}C_{82}]^{2-}$. The cage orientations are set to be identical to those shown in Figures 2, 4, and 6, respectively, to ease comparison. The 40 contour lines are in the range of 20 kcal/mol from the highest negative value of −135.08 kcal/mol for $[C_2(5)\text{-}C_{82}]^{2-}$, −136.26 kcal/mol for $[C_s(6)\text{-}C_{82}]^{2-}$, and −134.73 kcal/mol for $[C_{2v}(9)\text{-}C_{82}]^{2-}$, respectively.

Information, the metal positions in these three isomers are not changed after cocrystallization with Ni^{II}(OEP).

CONCLUSIONS

We have presented unambiguous crystallographic investigations of the three Yb@C_{82} isomers cocrystallized with Ni^{II}(OEP), unraveling their molecular structures as Yb@C_s(6)-C_{82} for Yb@C_{82}(I), Yb@C_2(5)-C_{82} for Yb@C_{82}(II), and Yb@C_{2v}(9)-C_{82} for Yb@C_{82}(III), respectively. The results from these crystallographic studies agree with the results of previous ^{13}C NMR studies that determined only the cage isomers present for these three endohedral metallofullerenes.[12] Moreover, we have found that the Yb^{2+} ion tends to be localized in some specific areas within the cages, regardless of the cage symmetry. These locations correspond to electrostatic potential minima and give the most stable configurations of these Yb@C_{82} isomers. Our results have enhanced the knowledge of the structures and properties of such less-explored divalent metallofullerenes and are helpful in understanding the unusual metal−cage interactions between a divalent metal ion and the popular C_{82} cages.

ASSOCIATED CONTENT

Supporting Information

Complete refs 5a, 6a, 6b, 7a, 7b, 8a, and 15; experimental details; optimized structures of Yb@C_2(5)-C_{82}, Yb@C_s(6)-C_{82}, and Yb@C_{2v}(9)-C_{82}; relationship between the respective Yb@C_{82} isomers and Ni^{II}(OEP); and X-ray crystallographic files in CIF format for Yb@C_2(5)-C_{82}·Ni^{II}(OEP)·2(benzene), Yb@C_s(6)-C_{82}·Ni^{II}(OEP)·2(benzene), and Yb@C_{2v}(9)-C_{82}·Ni^{II}(OEP)·2(benzene). This material is available free of charge via the Internet at http://pubs.acs.org.

AUTHOR INFORMATION

Corresponding Author

lux@mail.hust.edu.cn; nagase@ims.ac.jp; mmolmstead@ucdavis.edu; albalch@ucdavis.edu; akasaka@tara.tsukuba.ac.jp

Notes

The authors declare no competing financial interest.

ACKNOWLEDGMENTS

This work was supported by a Grant-in-Aid for Scientific Research on Innovative Areas (20108001, "π-Space"), Grants-in-Aid for Scientific Research (A) (202455006) and (B) (24350019), the Next Generation Super Computing Project (Nanoscience Project), the Nanotechnology Support Project, Grants-in-Aid for Scientific Research on Priority Area (20036008 and 20038007), a Specially Promoted Research Grant (22000009) from the Ministry of Education, Culture, Sports, Science, and Technology of Japan, and The Strategic Japanese−Spanish Cooperative Program funded by JST and MICINN. A.L.B. and M.M.O. thank the U.S. National Science Foundation (CHE-1011760 and CHE-0716843) for financial support. Generous support from The National Thousand Talents Program, The National Natural Science Foundation of China (21171061), and HUST to X.L. is gratefully acknowledged.

REFERENCES

(1) (a) *Endofullerenes: A New Family of Carbon Clusters*; Akasaka, T., Nagase, S., Eds.; Kluwer: Dordrecht, The Netherlands, 2002. (b) Yang, S.; Dunsch, L. Endohedral Fullerenes. In *Nanomaterials: Inorganic and Bioinorganic Perspectives*; Lukehart, C. M., Scott, R. A., Eds.; Wiley: Chichester, U.K., 2008; pp 189−214. (c) *Chemistry of Nanocarbons*; Akasaka, T., Wudl, F., Nagase, S., Eds.; Wiley-Blackwell: London, 2010. (d) Lu, X.; Akasaka, T.; Nagase, S. Rare Earth Metals Trapped inside Fullerenes—Endohedral Metallofullerenes. In *Rare Earth Coordination Chemistry: Fundamentals and Applications*; Huang, C. H., Ed.; Wiley: Singapore, 2010; pp 273−308.

(2) For recent reviews, see: (a) Dunsch, L.; Yang, S. *Small* **2007**, *3*, 1298−1320. (b) Chaur, M. N.; Melin, F.; Ortiz, A. L.; Echegoyen, L. A. *Angew. Chem., Int. Ed.* **2009**, *48*, 7514−7538. (c) Yamada, M.; Akasaka, T.; Nagase, S. *Acc. Chem. Res.* **2010**, *43*, 92−102. (d) Rodríguez-Fortea, A.; Balch, A. L.; Poblet, J. M. *Chem. Soc. Rev.* **2011**, *40*, 3551−3563. (e) Lu, X.; Akasaka, T.; Nagase, S. *Chem. Commun.* **2011**, *47*, 5942−5957. (f) Lu, X.; Feng, L.; Akasaka, T.; Nagase, S. *Chem. Soc. Rev.* **2012**, DOI: 10.1039/c2cs35214a. (g) Rivera-Nazario, D. M.; Pinzón, J. R.; Stevenson, S.; Echegoyen, L. A. *J. Phys. Org. Chem.* **2012**, DOI: 10.1002/poc.3009.

(3) Chai, Y.; Guo, T.; Jin, C. M.; Haufler, R. E.; Chibante, L. P. F.; Fure, J.; Wang, L. H.; Alford, J. M.; Smalley, R. E. *J. Phys. Chem.* **1991**, *95*, 7564−7568.

(4) Maeda, Y.; Tsuchiya, T.; Lu, X.; Takano, Y.; Akasaka, T.; Nagase, S. *Nanoscale* **2011**, *3*, 2421−2429.

(5) (a) Park, C. H.; et al. *Chem. Phys. Lett.* **1993**, *213*, 196−201. (b) Suenaga, K.; Iijima, S.; Kato, H.; Shinohara, H. *Phys. Rev. B* **2000**, *62*, 1627−1630. (c) Miyazaki, T.; Sumii, R.; Umemoto, H.; Okimoto, H.; Ito, Y.; Sugai, T.; Shinohara, H.; Hino, S. *Chem. Phys.* **2010**, *378*, 11−13.

(6) (a) Akasaka, T.; et al. *J. Am. Chem. Soc.* **2000**, *122*, 9316−9317. (b) Akasaka, T.; et al. *J. Phys. Chem. B* **2001**, *105*, 2971−2974.

(7) (a) Wakahara, T.; et al. *Chem. Phys. Lett.* **2002**, *360*, 235−239. (b) Wakahara, T.; et al. *J. Am. Chem. Soc.* **2004**, *126*, 4883−4887. (c) Feng, L.; Wakahara, T.; Tsuchiya, T.; Maeda, Y.; Lian, Y. F.;

Akasaka, T.; Mizorogi, N.; Kobayashi, K.; Nagase, S.; Kadish, K. M. *Chem. Phys. Lett.* **2005**, *405*, 274−277.
(8) (a) Maeda, Y.; et al. *J. Am. Chem. Soc.* **2004**, *126*, 6858−6859. (b) Lu, X.; Nikawa, H.; Tsuchiya, T.; Akasaka, T.; Toki, M.; Sawa, H.; Mizorogi, N.; Nagase, S. *Angew. Chem., Int. Ed.* **2010**, *49*, 594−597.
(9) (a) Yang, H.; Jin, H. X.; Zhen, H. Y.; Wang, Z. M.; Liu, Z. Y.; Beavers, C. M.; Mercado, B. Q.; Olmstead, M. M.; Balch, A. L. *J. Am. Chem. Soc.* **2011**, *133*, 6299−6306. (b) Yang, H.; Yu, M.; Jin, H.; Liu, Z.; Yao, M.; Liu, B.; Olmstead, M. M.; Balch, A. L. *J. Am. Chem. Soc.* **2012**, *134*, 5331−5338. (c) Jin, H. X.; Yang, H.; Yu, M. L.; Liu, Z. Y.; Beavers, C. M.; Olmstead, M. M.; Balch, A. L. *J. Am. Chem. Soc.* **2012**, *134*, 10933−10941.
(10) (a) Sato, S.; Nikawa, H.; Seki, S.; Wang, L.; Luo, G. F.; Lu, J.; Haranaka, M.; Tsuchiya, T.; Nagase, S.; Akasaka, T. *Angew. Chem., Int. Ed.* **2012**, *51*, 1589−1591. (b) Suzuki, M.; Lu, X.; Sato, S.; Nikawa, H.; Mizorogi, N.; Slanina, Z.; Tsuchiya, T.; Nagase, S.; Akasaka, T. *Inorg. Chem.* **2012**, *51*, 5270−5273.
(11) Yang, H.; Jin, H.; Wang, X.; Liu, Z.; Yu, M.; Zhao, F.; Mercado, B. Q.; Olmstead, M. M.; Balch, A. L. *J. Am. Chem. Soc.* **2012**, *134*, 14127−14136.
(12) Lu, X.; Slanina, Z.; Akasaka, T.; Tsuchiya, T.; Mizorogi, N.; Nagase, S. *J. Am. Chem. Soc.* **2010**, *132*, 5896−5905.
(13) Lu, X.; Lian, Y.; Beavers, C. M.; Mizorogi, N.; Slanina, Z.; Nagase, S.; Akasaka, T. *J. Am. Chem. Soc.* **2011**, *133*, 10772−10775.
(14) Sheldrick, G. M. *Acta Crystallogr.* **2008**, *A64*, 112−122.
(15) Frisch, M. J.; et al. *Gaussian 09*, revision A.02; Gaussian Inc.: Wallingford, CT, 2009.
(16) (a) Becke, A. D. *Phys. Rev. A* **1988**, *38*, 3098−3100. (b) Becke, A. D. *J. Chem. Phys.* **1993**, *98*, 5648−5652. (c) Lee, C.; Yang, W.; Parr, R. G. *Phys. Rev. B* **1988**, *37*, 785−789. (d) Cundari, T. R.; Stevens, W. J. *J. Chem. Phys.* **1993**, *98*, 5555−5565. (e) Cao, X. Y.; Dolg, M. *THEOCHEM* **2002**, *581*, 139−147. (f) Hay, P. J.; Wadt, W. R. *J. Chem. Phys.* **1985**, *82*, 299−310. (g) Hehre, W. J.; Ditchfield, R.; Pople, J. A. *J. Chem. Phys.* **1972**, *56*, 2257−2261. (h) Zhao, Y.; Truhlar, D. G. *Theor. Chem. Acc.* **2008**, *120*, 215−241.
(17) (a) Olmstead, M. M.; de Bettencourt-Dias, A.; Duchamp, J. C.; Stevenson, S.; Marciu, D.; Dorn, H. C.; Balch, A. L. *Angew. Chem., Int. Ed.* **2001**, *40*, 1223−1225. (b) Zuo, T. M.; Beavers, C. M.; Duchamp, J. C.; Campbell, A.; Dorn, H. C.; Olmstead, M. M.; Balch, A. L. *J. Am. Chem. Soc.* **2007**, *129*, 2035−2043.
(18) Sun, B. Y.; Sugai, T.; Nishibori, E.; Iwata, K.; Sakata, M.; Takata, M.; Shinohara, H. *Angew. Chem., Int. Ed.* **2005**, *44*, 4568−4571.
(19) Kroto, H. W. *Nature* **1987**, *329*, 529−531.